

Fluctuations at finite temperature and density

Szabolcs Borsányi[†]

Theoretical Physics, Bergische Universität Wuppertal, Gausstr 20, 42119 Wuppertal, Germany

E-mail: borsanyi@uni-wuppertal.de

Fluctuations of conserved charges in a grand canonical ensemble can be calculated as derivatives of the free energy with respect to the respective chemical potential. They are directly related to experimentally available observables that describe the hadronization in heavy ion collisions. The same derivatives can be used to extrapolate zero density results to finite chemical potential. We review the recent lattice calculations in the staggered formalism and discuss its implications to phenomenology and resummed perturbation theory.

The 33rd International Symposium on Lattice Field Theory

14 -18 July 2015

*Kobe International Conference Center, Kobe, Japan**

*Speaker.

[†]Wuppertal-Budapest collaboration

1. Introduction

In Quantum Chromodynamics (QCD) the net number of quarks in a closed system is conserved flavor by flavor. These conserved charges fluctuate in a grand canonical ensemble at finite temperature. The magnitude of these fluctuations are distinctly different in the hadronic and quark gluon plasma phases [1, 2]. In heavy ion experiments fluctuations appear in the event-by-event statistics of the net charges [3]. Continuum extrapolated lattice simulations with physical quark masses, that have already determined the QCD transition temperature [4, 5, 6, 7] and the equation of state [8, 9, 10], are now used to calculate these fluctuations in the grand canonical ensemble. The actual comparison of STAR data to lattice have placed the chemical freeze-out (i.e. the instant of the last inelastic scattering) at or slightly below the transition temperature [11]. Higher order baryon fluctuations are also indicators for the closeness of a critical end point [12].

From the theoretical point of view fluctuations are a proxy for the comparison between various theoretical and model approaches, such as the Hard Thermal Loop (HTL) perturbation theory at high temperature [13, 14, 15], the Hadron Resonance Gas (HRG) model in the confined phase [16, 17], or improved low energy models in the transition region [18].

Fluctuations are formally equivalent to the Taylor expansion coefficients of the free energy in a grand canonical ensemble. Thus, finite density methods open new ways to calculate these [19, 20]. On the other hand, the extrapolation of, for example, the equation of state to finite chemical potential is often a by-product of the calculation of generic fluctuations [21, 22]. The acute interest in small- μ physics was highlighted at this conference by four lattice groups presenting their results on the curvature of the chiral transition line in the QCD phase diagram [23, 24, 25, 26]. These results have been confronted to heavy ion data, where the experimentally observed fluctuations were matched to lattice data [27]. This comparison has shown a slight tension: the fluctuation data prefer a smaller (or even negative) curvature, which was also observed in a HRG-based calculation earlier [28]. The phase diagram at small chemical potential is likely to stay a hot topic at the coming Lattice and Quark Matter conferences.

In this work I review the recent progress of the fluctuation program on the lattice. Few years ago finite temperature results for the second order fluctuations became available in the continuum limit with physical quark masses [29, 30]. Since then, several higher order fluctuations have been continuum extrapolated, too, [31, 32, 33, 34, 35, 36]. Sophisticated combinations of higher order cross-correlators of conserved charges were also used to constrain the QCD spectrum in the strange [37] and in the charm sectors [38], as well as to study the pattern of melting of hadronic bound states [39, 40]. The papers cited in this paragraph were using staggered quarks. It must be said, that, although not yet with physical quark masses, second order fluctuations have already been calculated with Wilson quarks as well [41, 42, 43, 44, 19], a continuum limit was possible even in the overlap formulation [45].

I structured this presentation around five pillars: I am starting with the technical difficulties lattice groups face before a continuum extrapolated result can be obtained. Then I am presenting comparisons with the Hadron Resonance Gas model, and, in the following section, with improved perturbation theory. Then I am discussing the relations to non-zero density physics. Finally, since fluctuations are experimentally measured quantities a comparison between theory and experiment is presented.

2. Fluctuations on the lattice

The dimensionless fluctuations and correlators of quark numbers are the derivatives of the free energy (\sim pressure) with respect to the respective chemical potentials:

$$\chi_{i,j,k,l}^{u,d,s,c} = \frac{\partial^{i+j+k+l}(p/T^4)}{(\partial\hat{\mu}_u)^i(\partial\hat{\mu}_d)^j(\partial\hat{\mu}_s)^k(\partial\hat{\mu}_c)^l} \quad (2.1)$$

with $\hat{\mu}_q = \mu_q/T$. These are also called (generalized) susceptibilities.

χ_{11}^{ud} , for example, expresses the number of up quarks generated by an infinitesimal change in the down quark chemical potential $\hat{\mu}_d$ in a volume of T^{-3} . For this observable we present the lattice data of the Wuppertal-Budapest collaboration and the corresponding continuum limit in the left panel of Fig. 1, a continuum result that came 14 years after its first lattice computation [46]. Clearly, if light mesons (pions) dominate the thermodynamics at low temperature, one expects χ_{11}^{ud} to be zero at $T = 0$ and negative at $T \lesssim T_c$. As the T/M_{proton} ratio becomes non-negligible with increasing temperature light baryons (nucleons) will coexist with pions and the baryonic contribution will reverse the trend in $\chi_{11}^{ud}(T)$. The decoupling of quark flavors is one manifestation of deconfinement. In perturbation theory the correlation drops to zero as $\alpha^3 \log \alpha$. We will discuss the comparison to the HRG model in section 3 and study the high temperature behaviour in section 4.

Chemical potentials are introduced as imaginary, homogeneous, abelian A_0 fields on the lattice. Only the fermion determinant of the respective flavor depends on it. Thus, the observable D_j to be calculated is the j -th derivative of the logarithm of the fermion determinant (M), e.g. $D_1 = \frac{1}{4}\text{Tr}[M^{-1}dM/d\mu]$. (The factor 1/4 is only present for staggered fermions.) It is now straightforward to write down the lattice observable for the fluctuations. First we remark, that $\chi_1^u(T) \sim d\log Z/d\mu_u \sim \langle D_1^u \rangle$ is zero at vanishing chemical potential due to the \mathcal{C} -symmetry, and the same holds for all odd derivatives.

$$\chi_2^u = \frac{1}{TV} [\langle D_1^u D_1^u \rangle - \langle D_1^u \rangle \langle D_1^u \rangle + \langle D_2^u \rangle], \quad (2.2)$$

$$\chi_{11}^{ud} = \frac{1}{TV} [\langle D_1^u D_1^d \rangle - \langle D_1^u \rangle \langle D_1^d \rangle]. \quad (2.3)$$

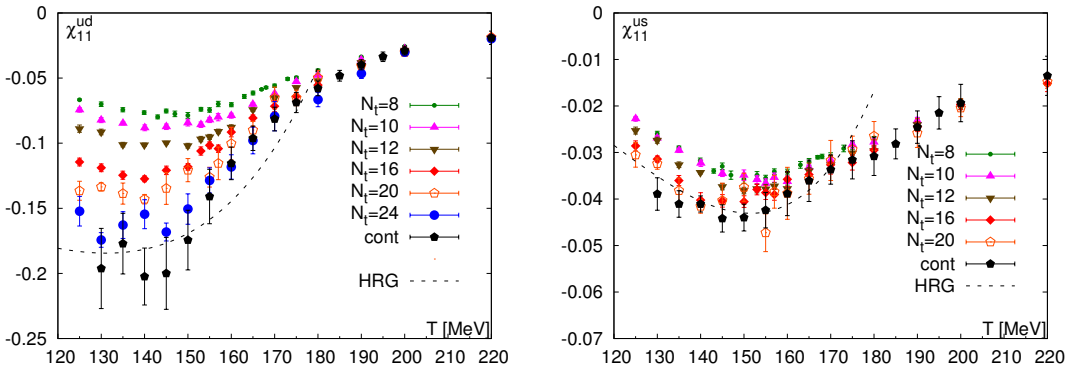


Figure 1: The up-down correlator (χ_{11}^{ud}) for a range of lattice spacings using the 4stout staggered action of the Wuppertal-Budapest group [35]. We also show the light-strange correlator (χ_{11}^{us}) in the right panel, for comparison.

In other words, if we assume degenerate up and down quarks (and no dynamical QED effects), then χ_{11}^{ud} will be the disconnected part of the light quark number susceptibilities. The traces in the D_j contributions are typically calculated using Gaussian random sources, excluding, of course, those contributions from $\langle D_1^u D_1^u \rangle$ where both traces were estimated using the same random source. For details, see Refs. [46, 47] or the more recent [35, 36].

Notice the strong lattice spacing dependence in Fig. 1. The Wuppertal-Budapest group has gone as far as including $N_t = 24$ lattices into the continuum extrapolation. At the heart of the discretization errors there is the typically slow approach of the staggered pions to the physical spectrum. Observables, like $\chi_2^u + \chi_{11}^{ud}$, on the other hand, are related to light baryon fluctuations and have a more favourable continuum scaling.

It was pointed out in Ref. [47] that the odd D_j coefficients are the Taylor coefficients of the phase of the fermion determinant $\det M = |\det M|e^{i\theta}$:

$$\theta = N_f \text{Im} \left[\frac{\mu_B}{3} D_1 + \frac{\mu_B^3}{3^3 \cdot 3!} D_3 + \dots \right] \quad (2.4)$$

where N_f are the number of flavors for which the chemical potential is introduced. With the choice of $N_f = 2$ light quarks we have

$$\langle e^{i\theta} \rangle = 1 + \frac{2}{9} \mu_B^2 V T \chi_{11}^{ud} + \mathcal{O}(\mu_B^4). \quad (2.5)$$

This clearly shows, that the severity of the sign problem for small chemical potentials is basically set by χ_{11}^{ud} . Notice that staggered lattice artefacts, actually, greatly ease the sign problem. Closer to the continuum limit, $\chi_{11}^{ud} \approx -0.2$, to leading order $\langle e^{i\theta} \rangle = 0.5$ is reached at $\mu_B = 184, 100, 65$ MeV for an aspect ratio of $LT = 2, 3$ and 4 , respectively.

The connected contribution $\langle D_2^u \rangle$ in Eq. 2.2 is proportional to the isospin fluctuations. Being dominated by pions at low temperature, this quantity shows the same (absolute) discretization errors as χ_{11}^{ud} . This difficulty, however, can be overcome by switching to a chiral representation of fermions. This has been done in Ref. [45], showing results with two dynamical flavors with $M_\pi = 350$ MeV, (see Fig. 2).

The continuum scaling for higher order fluctuations are under control at high temperatures (see Fig. 3). Around and below the transition temperature lattice calculations face two challenges: the fourth moment of the electric charge fluctuation has strong lattice artefacts with all known staggered actions, thus finer lattices are needed. On the other hand, higher order baryon fluctuations are very noisy at low T , especially on fine lattices, where disconnected contributions are not suppressed by lattice artefacts (see Fig. 1). Disconnected parts come with less noise in smaller volumes. However, finite volume effects can be present in the continuum, even though they are often hidden at finite N_t because of the same lattice artefacts.

3. Fluctuations and the Hadron Resonance Gas model

At low temperatures QCD can be modelled as a gas of uncorrelated hadrons, where interactions are included as a tower of resonances. These states are taken from the Particle Data Book

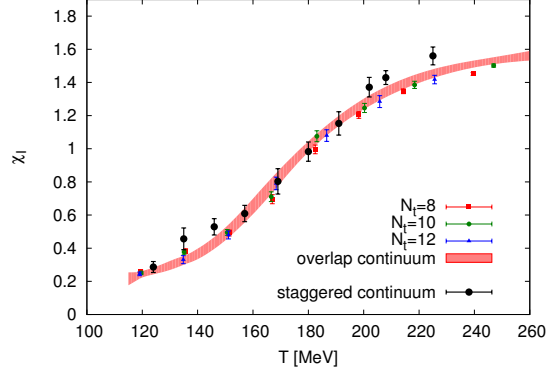


Figure 2: Continuum extrapolation of the isospin fluctuations in an $N_f = 2$ theory with $M_\pi = 350$ MeV using chiral fermions. The staggered result is also continuum extrapolated and corresponds to the same theory [45].

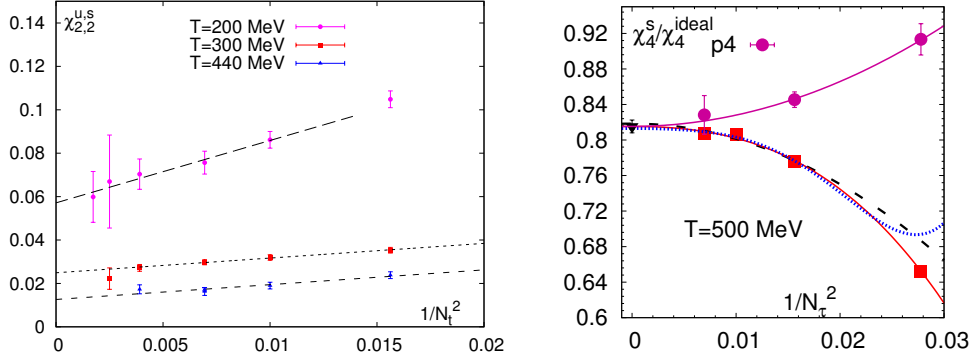


Figure 3: Continuum scaling of the off-diagonal and diagonal higher order fluctuations. On the left panel we show $\chi_{2,2}^{us}$ for the 4stout staggered action of the Wuppertal-Budapest group [45], the right panel shows the scaling of the HISQ and p4 actions for χ_4^s by the BNL group [36].

[48]. The pressure of the Hadron Resonance Gas reads

$$\frac{p^{\text{HRG}}}{T^4} = \frac{1}{VT^3} + \sum_{i \in \text{mesons}} \log \mathcal{L}^M(T, V, m_i, \{\mu\}) + \sum_{i \in \text{baryons}} \log \mathcal{L}^B(T, V, m_i, \{\mu\}) \quad (3.1)$$

with

$$\log \mathcal{L}_{m_i}^{M/B} = \mp \frac{V d_i}{2\pi^2} \int_0^\infty dk k^2 \log \left(1 \mp z_i e^{-\sqrt{m_i^2 + k^2}/T} \right) \quad (3.2)$$

$$= \frac{VT^3}{2\pi^2} d_i \frac{m_i^2}{T^2} \sum_{k=1}^\infty (\pm)^{k+1} \frac{z_i^k}{k^2} K_2(km_i/T), \quad (3.3)$$

with the fugacity factor $z_i = \exp(B_i \hat{\mu}_B + Q_i \hat{\mu}_Q + S_i \hat{\mu}_S)$, the degeneracy factor d_i and $\hat{\mu} = \mu/T$.

In HRG as well as in phenomenology it is more convenient to work in the $B - Q - S$ base, already used in Eq. (3.3). These refer to the baryon number, electric charge and strangeness, the

corresponding chemical potentials are defined by the following equations:

$$\mu_u = \frac{1}{3}\mu_B + \frac{2}{3}\mu_Q, \quad \mu_d = \frac{1}{3}\mu_B - \frac{1}{3}\mu_Q, \quad \mu_s = \frac{1}{3}\mu_B - \frac{1}{3}\mu_Q - \mu_S. \quad (3.4)$$

The six second order derivatives in the $B - Q - S$ base are mapped into the $u - d - s$ base where due to the $u \leftrightarrow d$ degeneracy of the lattice setup only four derivatives are different:

$$\chi_2^u = 2\chi_2^B + \chi_2^Q + \chi_{11}^{BS}, \quad (3.5)$$

$$\chi_2^s = \chi_2^S, \quad (3.6)$$

$$\chi_{11}^{ud} = \frac{5}{2}\chi_2^B - \chi_2^Q + \frac{1}{2}\chi_2^S + 2\chi_{11}^{BS}, \quad (3.7)$$

$$\chi_{11}^{us} = -\frac{1}{2}\chi_2^S - \frac{3}{2}\chi_{11}^{BS} = -3\chi_{11}^{QS} + \chi_2^S = \frac{3}{2}\chi_2^B - \frac{1}{2}\chi_2^S - 3\chi_{11}^{BQ}, \quad (3.8)$$

The first comparison between lattice and HRG has already been shown in Fig. 1. The two panels show an agreement both for the light-light and the light-strange correlators, yet the highest temperature where the hadronic description is consistent with data is slightly higher for the strange at the level of this precision. The differences between light and strange sectors have been put to a less ambiguous test. Certain combinations of derivatives are constant zero (or = 1) in HRG, independently of the resonance list in use, but are non-zero (or $\neq 1$) if quarks are free. These typically involve the difference (or ratio) of correlators with different order of baryon derivative. For baryons, typically only the $k = 1$ term contributes significantly in Eq. (3.3), neglecting $k \neq 1$ is called the Boltzmann approximation. In this limit the contribution of each resonance of mass m_i and its antiparticle to the QCD pressure is

$$\frac{p}{T^4} = 2d_i \frac{VT^3}{2\pi^2} \frac{m_i^2}{T^2} K_2(m_i/T) \cosh(B_i \hat{\mu}_B + Q_i \hat{\mu}_Q + S_i \hat{\mu}_S), \quad (3.9)$$

where B_i , Q_i and S_i are integer quantum numbers. For an ideal gas, on the other hand, the pressure at finite chemical potential reads [49]

$$\frac{p}{T^4} = \frac{8\pi^2}{45} + \frac{7\pi^2}{60} N_f + \frac{1}{2} \sum_f \left(\frac{\mu_f^2}{T^2} + \frac{\mu_f^4}{2\pi^2 T^4} \right). \quad (3.10)$$

There are combinations of fluctuations that have a non-zero Stefan-Boltzmann limit but vanish in the HRG approach:

$$\chi_4^B - \chi_2^B = 0, \quad (3.11)$$

$$v_1 = \chi_{31}^{BS} - \chi_{11}^{BS} = 0, \quad (3.12)$$

$$v_2 = \frac{1}{3}(\chi_2^S - \chi_4^S) - 2\chi_{13}^{BS} - 4\chi_{22}^{BS} - 2\chi_{31}^{BS} = 0. \quad (3.13)$$

Thus, these can be considered as indicators for deconfinement. Others, $\chi_{11}^{BC}/\chi_{13}^{BC}$, $\chi_{31}^{BS}/\chi_{11}^{BS}$ and $\chi_{31}^{BQ}/\chi_{11}^{BQ}$ are always = 1 in the confined phase. We show the results for these combinations in Fig. 4 using the $N_f = 8$ data of the BNL-Bielefeld group. Notice that both $\chi_2^B - \chi_4^B$ and $\chi_{31}^{BQ}/\chi_{11}^{BQ}$ are dominated by the light flavors. The plots in Fig. 4 suggests a slight flavor dependence in the deconfinement pattern. In Ref. [33] the Wuppertal-Budapest group has presented the light counterparts of v_1 and v_2 , showing a slight difference between flavors.

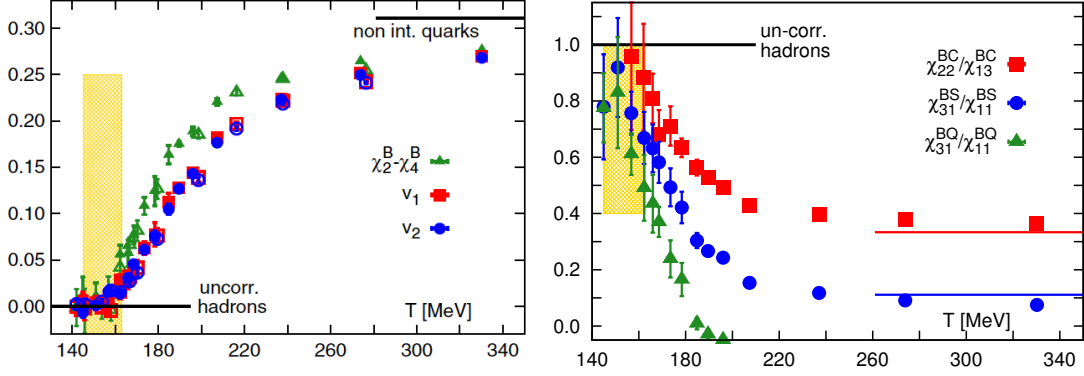


Figure 4: Combinations of generalized susceptibilities that are constant 0 (left panel) or 1 (right panel) within the Hadron Resonance Gas model for any list of resonances. Calculating these in full QCD the departure of these curves from the hadronic expectation provides for a flavor dependent indicator of deconfinement. On the right hand side the horizontal lines show the Stefan-Boltzmann limit according to Eq. (3.10). Here we show the plots by the BNL-Bielefeld group [39, 38].

4. Fluctuations and improved perturbation theory

In the high temperature limit perturbation theory gives an appropriate description of QCD. The pressure at zero chemical potential is known up to $\alpha^3 \log(\alpha)$ order [50], which was extended to $\mu_B > 0$ in [51, 52]. Combining these findings with the dimensional reduction [53] recently estimates for the four-loop perturbative quark number susceptibilities have emerged [54, 55].

The reorganization of the perturbative series around hard thermal loops also improves the convergence [13, 15]. This was exploited in full QCD in Refs. [56, 57]. For the fluctuations subsequent orders have been calculated in Refs. [14, 58, 54, 59, 60]. These developments allowed the HTL calculation of the equation of state at finite chemical potentials [61].

We expect that at several T_c temperature these diagrammatic approaches agree among themselves and are consistent with lattice. To find out the range of validity both the Wuppertal-Budapest and BNL groups have conducted high temperature simulations and calculated generalized quark number susceptibilities in the continuum limit [31, 35, 34, 36].

In the left panel of Fig. 5 we show χ_2 for the light quark as well as for the baryons. The Wuppertal-Budapest data is based on the 4stout action [35], the BNL-Bielefeld result is using the HISQ action (in combined analysis with p4 data) [34].

The off-diagonal susceptibilities (already shown in Fig. 1) are compared to the leading log result in right panel of Fig. 5. The magnitude of the Hadron Resonance Gas result on χ_{11} is two orders of magnitude higher the perturbative estimate ($\sim \alpha^3 \log(\alpha)$), which is reached at about $3T_c$ temperature by the lattice data. It is remarkable that even the charm-up correlator is consistent with the perturbative result in the temperature range accessible to simulations. Below $3T_c$ the charm is practically uncorrelated with the other quarks. The mass of the strange quark becomes negligible near $1.5T_c$.

Finally we show the diagonal and off-diagonal fourth order correlators. In Fig. 6 we show χ_4^U on the left panel and both the light-light and the light-strange correlators (χ_{22}) on the right

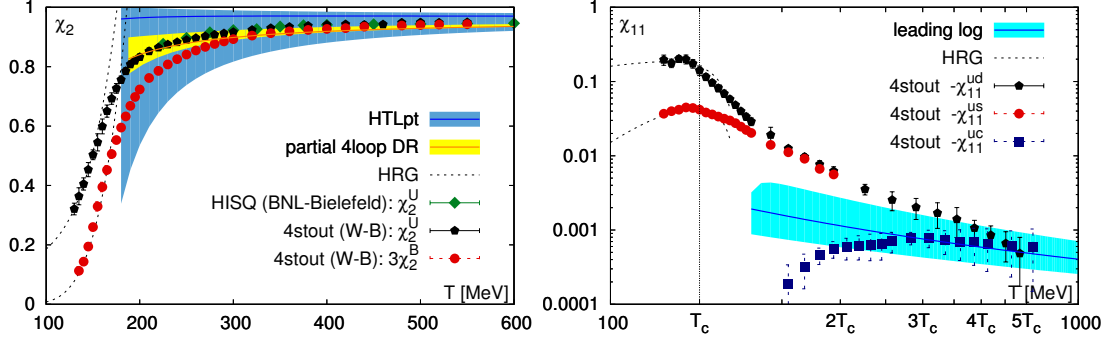


Figure 5: Left: The (diagonal) light quark number susceptibility χ_2^U and the baryon susceptibility χ_2^B at high temperatures [35, 34]. We also show the latest (improved) perturbative results with Hard Thermal Loops (HTL) [60] and dimensional reduction (DR) [55]. Right: The (off-diagonal) quark correlators between the light quark and the light (black), strange (red) and charm (blue) quarks. The light-light correlator spans more than two orders of magnitude in the temperature range between T_c and $5T_c$. The leading $\mathcal{O}(\alpha^3 \log \alpha)$ perturbative result comes from Ref. [14].

panel. Here the effect of the strange mass diminishes already at around 200 MeV temperature. The agreement with the HTL result starts at a low temperature because of the large uncertainties, the central line is approached at $T \sim 250$ MeV. We also show the prediction of dimensional reduction [55], though for χ_{22} it is not in agreement with HTL, nor with the lattice data.

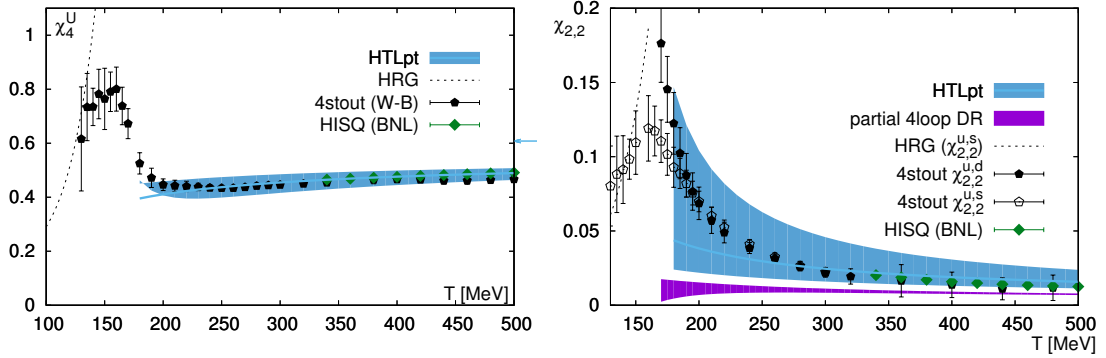


Figure 6: The diagonal (left) and off-diagonal (right) fourth order fluctuation at high temperature. We compare the continuum result of two collaborations: Wuppertal-Budapest [35] and BNL [36]. The shown off-diagonal derivative is the only one with a non-vanishing contribution in three-loop HTL [61]. The dimensional reduction (DR) data set is from Ref. [55].

5. Fluctuations and physics at non-zero chemical potential

Fluctuations naturally give access to the physics at small chemical potential. The definition of the generalized susceptibilities (χ) in Eq. (2.1) immediately connect the Taylor coefficients

of the QCD pressure to the baryon fluctuations. Continuum results have been calculated by the Wuppertal-Budapest group as well as the HotQCD collaboration to leading order [29, 30], to next-to-leading order the Wuppertal-Budapest group published Refs. [32, 35].

For the calculation of the equation of state at small chemical potential for the phenomenological use we still need to add one ingredient. Since there is no net strangeness in the colliding nuclei, and the strangeness is conserved, the expectation value of the net strangeness is zero in experiment. This must be reflected in the grand canonical ensemble that we are using to calculate the bulk thermodynamics of the plasma.

Thus a pair of equations can be set up and solved, requiring that at any finite chemical potential

$$\chi_1^S(\mu_B, \mu_Q, \mu_S) = 0, \quad \chi_1^B(\mu_B, \mu_Q, \mu_S) = \frac{Z}{A} \chi_1^Q(\mu_B, \mu_Q, \mu_S). \quad (5.1)$$

These two equations connect the electric charge and strangeness chemical potentials to the baryon chemical potential, which have been calculated to next-to-leading order using fourth-order fluctuations [62, 32] and for imaginary chemical potentials [24].

The first continuum result for the leading order Taylor expansion (already implementing strangeness neutrality) was published in Ref. [21]. The BNL-Bielefeld group has presented the next orders with $N_f = 8$ HISQ fermions [22]. In Fig. 7 we show the fourth order coefficient: on the left panel the BNL-Bielefeld result, on the right panel the preliminary continuum result of the Wuppertal-Budapest group, based on $N_f = 8, 10, 12$ and 16 lattices (as of the Quark Matter conference in 2015).

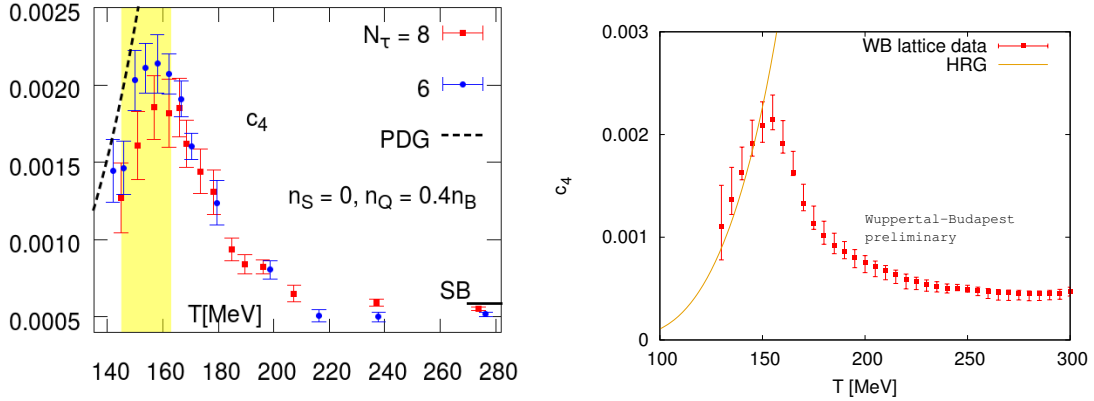


Figure 7: Preliminary μ_B^4 order Taylor coefficient of the QCD pressure. Left: BNL-Bielefeld group ($N_f = 8$) [22], right: Wuppertal-Budapest group (continuum). The errors are only statistical.

Besides the equation of state the χ coefficients can also extrapolate the quark number susceptibilities to finite chemical potentials. The inflection point of the strange susceptibility is one possible estimator of the deconfinement transition. In Fig. 8 we show $\chi_2^S(T)$ extrapolated to an imaginary value of the chemical potential, where direct simulations are also possible. The extrapolation is to leading (χ_B^2) order. The intrinsic periodicity in the imaginary part of μ_B restricts the range of independent simulation points to $0 \leq \text{Im}\mu_B \leq \pi T$. In Fig. 8 the leading order expansion gives accurate result in more than half of the available interval.

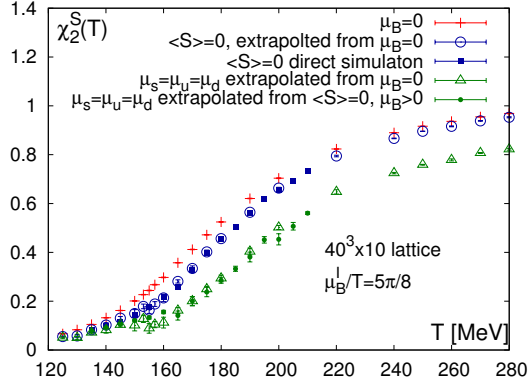


Figure 8: Strange susceptibility at vanishing (red) and non-vanishing (imaginary) chemical potentials on a $40^3 \times 10$ lattice with the 4stout action. The blue squares are the direct simulation points at μ_B, μ_S pairs where the net strangeness vanishes. These data are reproduced by a leading Taylor estimate (open circles). If we keep all chemical potentials equal instead of requiring strangeness neutrality we arrive at the green dots and triangles. The latter two refer to an extrapolation from the $\mu_B = 0$ or the $\text{Im}\mu_B > 0$ data, they are in agreement [24].

The strange susceptibility together with the chiral condensate and susceptibility was used to calculate the curvature of the transition line in the QCD phase diagram [63]. The use of imaginary chemical potentials became a very popular approach, since then the μ_B -derivative of the chiral observables do not have to be calculated. Instead, T_c has to be determined for several imaginary values of the chemical potentials. Recently three consistent continuum results emerged [23, 24, 25]. In Fig. 9 we show the continuum extrapolated T_c results at various imaginary chemical potentials and the phase diagram after the analytical continuation. The curvature κ of the phase diagram is defined as

$$\frac{T_c(\mu_B)}{T_c(\mu=0)} = 1 - \kappa \left(\frac{\mu_B}{T_c(\mu_B)} \right)^2 + \mathcal{O}(\mu_B^4). \quad (5.2)$$

The Pisa group concluded at $\kappa = 0.0135(15)$ (2stout staggered action up to $N_t = 12$) [23] the Wuppertal-Budapest group published $\kappa = 0.0149(21)$ (4stout staggered action up to $N_t = 16$) [24].

6. Fluctuations, where theory meets experiment

Perhaps the most beautiful aspect of fluctuations of conserved charges is their availability from heavy ion experiments. Fluctuations are characteristic to the temperature, chemical potential(s) and volume of a grand canonical ensemble. Using a somewhat simplified picture, the plasma that was created at a high energy density equilibrates locally and follows a hydrodynamical evolution, simultaneously cooling down into the transition range. Although the total baryon number and electric charge are conserved a subsystem can be described by a grand canonical ensemble, though it is important to consider the finite size of the subvolume [72]. The net abundance of conserved charges in a subsystem is counted by using rapidity cuts in experiment. The efficiency of the detector is corrected for and spallation protons are excluded by appropriate cuts in p_T , though such cuts also introduce systematic errors [73]. At RHIC STAR has published results on the first

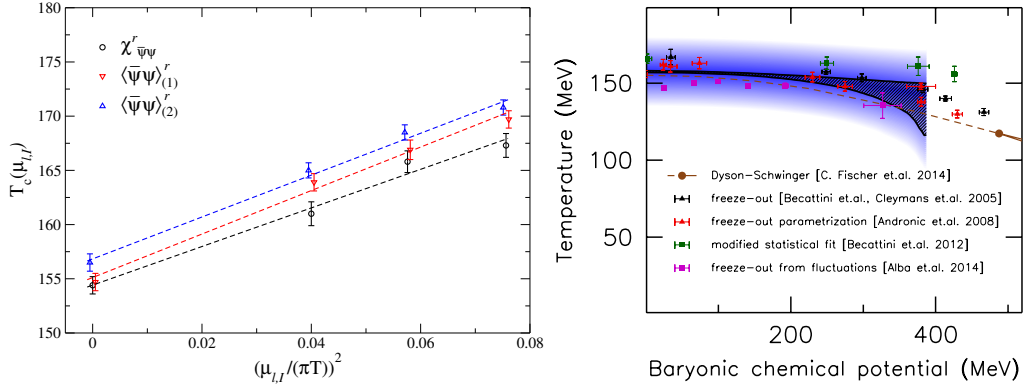


Figure 9: Left: continuum extrapolated chiral T_c results at imaginary chemical potentials by the Pisa group [23]. Right: the analytical continuation Wuppertal-Budapest group (continuum). The errors are only statistical. For comparison, we show on the right panel a selection of non-lattice results: from Dyson-Schwinger equations in Ref. [64] and from the phenomenological fitting of experimental freeze-out data in Refs. [65, 66, 67, 68, 69, 70, 71]

four moments of the net proton [74] as well as net-electric charge [75] event-by-event fluctuations. Both STAR and PHENIX have presented further preliminary results at the Quark Matter (2015) conference. These experiments are part of the beam energy scan program [76], which spans the energy range between 200 and 7.7 GeV center-of-mass beam energies, with a new run $\sqrt{s_{NN}} = 14.5$ added this year.

The direct comparison between fluctuations on the lattice and in experiment have known caveats. First, one assumes the validity of the grand canonical description in equilibrium. The size (V) of the detected subsystem is an unknown, the measured mean ($M \sim V\chi_1$), variance ($\sigma^2 \sim V\chi_2$) skewness ($S \sim V^{-1/2}\chi_3/\chi_2^{3/2}$) and kurtosis ($\kappa \sim V^{-1}\chi_4/\chi_2^2$) all carry a power of V as a prefactor. Forming ratios

$$\begin{aligned} S\sigma &= \chi_3/\chi_2 & ; & & \kappa\sigma^2 &= \chi_4/\chi_2 \\ M/\sigma^2 &= \chi_1/\chi_2 & ; & & S\sigma^3/M &= \chi_3/\chi_1 \end{aligned} \quad (6.1)$$

the volume can be cancelled, though a residual V dependence may persist as a sensitivity of these ratios to the rapidity cut. A further source of systematics is that V is not constant, its event-by-event fluctuation mixes into the measured ratios [77, 78].

Nevertheless, we can assume for now, that the fluctuations in experiment are described by a grand canonical ensemble, that corresponds to the last hyper-surface of inelastic scatterings, the chemical freeze-out. After this the conserved charges are indeed conserved also in the sub-system, that is finally detected, and its event-by-event fluctuations can be matched to the QCD prediction. This matching means that a pair of equations are solved, e.g. [30]

$$M/\sigma^2|_{\text{experiment}} = \chi_1(T, \mu_B)/\chi_2(T, \mu_B)|_{\text{lattice}} , \quad (6.2)$$

$$S\sigma^3/M|_{\text{experiment}} = \chi_3(T, \mu_B)/\chi_1(T, \mu_B)|_{\text{lattice}} . \quad (6.3)$$

This was applied to the electric and baryon charges [30, 32, 11]. In experiment proton fluctuations are measured instead of full baryon fluctuations, this introduces further systematics [79].

In Eqs. (6.2-6.3) lattice data are needed at finite chemical potential. These we can have by Taylor-expanding the fluctuations and use only the highest collision energies (corresponding to small μ_B). The extrapolation is in all chemical potentials such that Eqs. (5.1) are always fulfilled. At the level of our current precision the small curvature (κ) means that the transition temperature is constant within two MeV for central collisions with $\sqrt{s_{NN}} \gtrsim 27$ GeV (see section 5), the chemical freeze-out temperature is expected to behave likewise.

In Fig. 10 we present the M/σ ratio for the baryon number (left) and the electric charge (right). The experimental data on M/σ^2 selects a possible range of chemical potentials where the freeze-out occurred. The shown temperatures span the range preferred by the skewness data [11]. The chemical potentials from the matching of both data sets to lattice are shown in Fig. 11. Along with the μ_B from the Wuppertal-Budapest analysis we show the result of the Statistical Hadronization Model [80, 67]. The latter method is the standard procedure for phenomenological determination of the freeze-out curve, it compares particle yield ratios to experiment on the basis of the Hadron Resonance Gas model. Its result is shown with triangles in Fig. 9. For a similar HRG-based fluctuation analysis see Ref. [71].

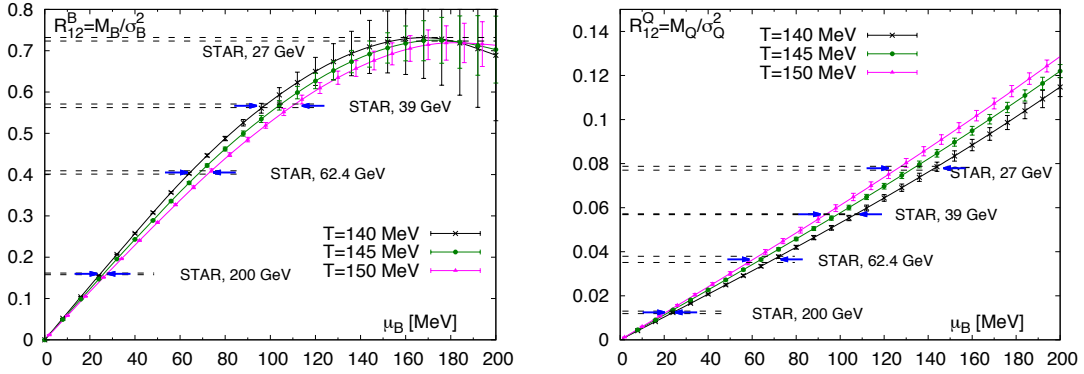


Figure 10: χ_1^B/χ_2^B (left) and χ_1^Q/χ_2^Q (right) as a function of the chemical potential using μ_B^3 order Taylor expansion. The STAR data are from Refs. [74, 75] using the two most central bins (0-10%) [11].

A remarkable feature in Fig. 11 is the agreement between the two fluctuation data sets and also between the SHM and the fluctuation approach. This shows the robustness of fluctuations despite the already discussed systematic effects. We note that SHM gives higher temperatures than the fluctuation method (either with HRG or with lattice), this can also be seen in Fig. 9. Notice that the freeze-out temperatures obtained in the SHM model analysis are in a range where lattice and HRG model are no longer in agreement. The non-monotonicity in Ref. [71] may hint at systematic effects that have to be understood in the future. A recent contribution in this direction calculates the curvature of the freeze-out line based on the comparison of lattice to latest STAR data [27]. Though its result is still consistent with the curvature of the chiral transition line, data prefer a negative value. As lattice data become increasingly accurate the subtle phenomenological details of the matching between theory and experiment must be better studied.

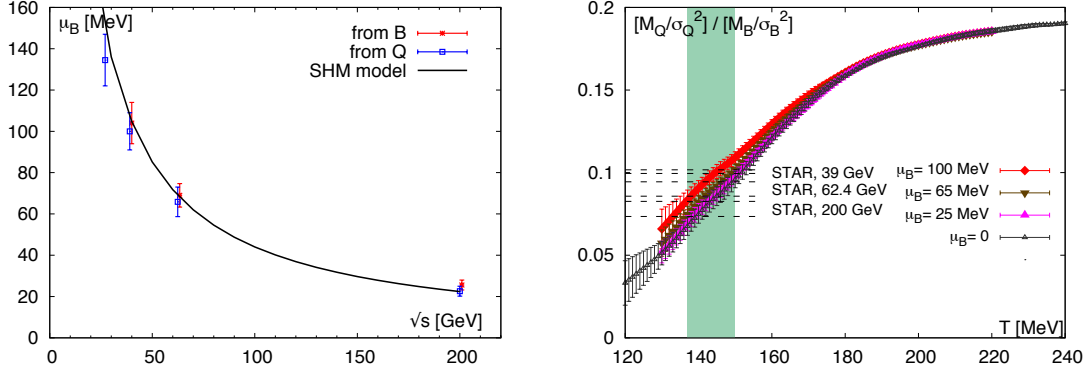


Figure 11: Left: comparison of the chemical potentials coming from the freeze-out analysis to the statistical hadronization model [80]. There is consistency between the baryon and charge-based observables. If we now assume that M/σ correspond to the same (T, μ_B) parameters then a thermometer can be constructed from this ratio, which, in turn is compatible with experimental data only if freeze-out occurred in the transition region, marked with the green band [11].

Acknowledgement

This summary is based on my work in collaboration with R. Bellwied, Z. Fodor, J. Günther, S. D. Katz, S. Krieg, A. Pásztor, C. Ratti and K. K. Szabó. The numerical simulations were performed on the QPACE machine, the GPU cluster at the Wuppertal University, and on JUQUEEN (the Blue Gene/Q system of the Forschungszentrum Juelich) and on MIRA at the Argonne Leadership Computing Facility through the Innovative and Novel Computational Impact on Theory and Experiment (INCITE) program of the U.S. Department of Energy (DOE).

References

- [1] S. Jeon and V. Koch, *Phys.Rev.Lett.* **85**, 2076 (2000).
- [2] M. Asakawa, U. W. Heinz, and B. Muller, *Phys.Rev.Lett.* **85**, 2072 (2000).
- [3] X. Luo, *J.Phys.Conf.Ser.* **599**, 012023 (2015).
- [4] Y. Aoki, Z. Fodor, S. Katz, and K. Szabo, *Phys.Lett.* **B643**, 46 (2006).
- [5] Y. Aoki *et al.*, *JHEP* **0906**, 088 (2009).
- [6] Wuppertal-Budapest Collaboration, S. Borsanyi *et al.*, *JHEP* **1009**, 073 (2010).
- [7] A. Bazavov *et al.*, *Phys.Rev.* **D85**, 054503 (2012).
- [8] S. Borsanyi *et al.*, *JHEP* **1011**, 077 (2010).
- [9] S. Borsanyi *et al.*, *Phys.Lett.* **B730**, 99 (2014).
- [10] HotQCD Collaboration, A. Bazavov *et al.*, *Phys.Rev.* **D90**, 094503 (2014).
- [11] S. Borsanyi *et al.*, *Phys.Rev.Lett.* **113**, 052301 (2014).
- [12] M. A. Stephanov, K. Rajagopal, and E. V. Shuryak, *Phys.Rev.* **D60**, 114028 (1999).

- [13] E. Braaten and R. D. Pisarski, Phys.Rev. **D45**, 1827 (1992).
- [14] J. Blaizot, E. Iancu, and A. Rebhan, Phys.Lett. **B523**, 143 (2001).
- [15] J. O. Andersen, E. Braaten, E. Petitgirard, and M. Strickland, Phys.Rev. **D66**, 085016 (2002).
- [16] R. Dashen, S.-K. Ma, and H. J. Bernstein, Phys.Rev. **187**, 345 (1969).
- [17] R. Venugopalan and M. Prakash, Nucl.Phys. **A546**, 718 (1992).
- [18] W.-j. Fu and J. M. Pawłowski, (2015), 1508.06504.
- [19] C. Gattringer and H.-P. Schadler, Phys.Rev. **D91**, 074511 (2015).
- [20] R. Fukuda, A. Nakamura, and S. Oka, (2015), 1504.06351.
- [21] S. Borsanyi *et al.*, JHEP **1208**, 053 (2012).
- [22] BNL-Bielefeld-CCNU, P. Hegde, PoS **LATTICE2014**, 226 (2014).
- [23] C. Bonati *et al.*, Phys. Rev. **D92**, 054503 (2015).
- [24] R. Bellwied *et al.*, (2015), 1507.07510.
- [25] P. Cea, L. Cosmai, and A. Papa, (2015), 1508.07599.
- [26] for the Bielefeld-BNL-CCNU, P. Hegde and H.-T. Ding, PoS **LATTICE2015**, 141 (2015).
- [27] A. Bazavov *et al.*, (2015), 1509.05786.
- [28] P. Alba *et al.*, J.Phys.Conf.Ser. **599**, 012021 (2015).
- [29] S. Borsanyi *et al.*, JHEP **1201**, 138 (2012).
- [30] HotQCD Collaboration, A. Bazavov *et al.*, Phys.Rev. **D86**, 034509 (2012).
- [31] S. Borsanyi, Nucl.Phys. **A904-905**, 270c (2013).
- [32] S. Borsanyi *et al.*, Phys.Rev.Lett. **111**, 062005 (2013).
- [33] R. Bellwied, S. Borsanyi, Z. Fodor, S. D. Katz, and C. Ratti, Phys.Rev.Lett. **111**, 202302 (2013).
- [34] A. Bazavov *et al.*, Phys.Rev. **D88**, 094021 (2013).
- [35] R. Bellwied *et al.*, (2015), 1507.04627.
- [36] H. T. Ding, S. Mukherjee, H. Ohno, P. Petreczky, and H. P. Schadler, Phys. Rev. **D92**, 074043 (2015).
- [37] A. Bazavov *et al.*, Phys.Rev.Lett. **113**, 072001 (2014).
- [38] A. Bazavov *et al.*, Phys.Lett. **B737**, 210 (2014).
- [39] A. Bazavov *et al.*, Phys. Rev. Lett. **111**, **082301**, 082301 (2013).
- [40] S. Mukherjee, P. Petreczky, and S. Sharma, (2015), 1509.08887.
- [41] S. Borsanyi *et al.*, JHEP **1208**, 126 (2012).
- [42] S. Borsanyi *et al.*, (2015), 1504.03676.
- [43] P. Giudice *et al.*, PoS **LATTICE2013**, 492 (2014).
- [44] G. Aarts *et al.*, JHEP **1502**, 186 (2015).
- [45] S. Borsanyi *et al.*, (2015), 1510.03376.
- [46] R. V. Gavai, S. Gupta, and P. Majumdar, Phys.Rev. **D65**, 054506 (2002).

- [47] C. Allton *et al.*, Phys.Rev. **D66**, 074507 (2002).
- [48] Particle Data Group, K. A. Olive *et al.*, Chin. Phys. **C38**, 090001 (2014).
- [49] J. I. Kapusta and C. Gale, *Finite-Temperature Field Theory*, Second ed. (Cambridge University Press, 2006), Cambridge Books Online.
- [50] K. Kajantie, M. Laine, K. Rummukainen, and Y. Schroder, Phys.Rev. **D67**, 105008 (2003).
- [51] A. Vuorinen, Phys.Rev. **D68**, 054017 (2003).
- [52] A. Ipp, K. Kajantie, A. Rebhan, and A. Vuorinen, Phys.Rev. **D74**, 045016 (2006).
- [53] J. Blaizot, E. Iancu, and A. Rebhan, Phys.Rev. **D68**, 025011 (2003).
- [54] J. O. Andersen, S. Mogliacci, N. Su, and A. Vuorinen, Phys.Rev. **D87**, 074003 (2013).
- [55] S. Mogliacci, J. O. Andersen, M. Strickland, N. Su, and A. Vuorinen, JHEP **1312**, 055 (2013).
- [56] M. Strickland, J. O. Andersen, L. E. Leganger, and N. Su, Prog.Theor.Phys.Suppl. **187**, 106 (2011).
- [57] J. O. Andersen, L. E. Leganger, M. Strickland, and N. Su, Phys.Rev. **D84**, 087703 (2011).
- [58] J. Blaizot, E. Iancu, and A. Rebhan, Eur.Phys.J. **C27**, 433 (2003).
- [59] N. Haque, M. G. Mustafa, and M. Strickland, JHEP **1307**, 184 (2013).
- [60] N. Haque, J. O. Andersen, M. G. Mustafa, M. Strickland, and N. Su, Phys.Rev. **D89**, 061701 (2014).
- [61] N. Haque *et al.*, JHEP **1405**, 027 (2014).
- [62] A. Bazavov *et al.*, Phys.Rev.Lett. **109**, 192302 (2012).
- [63] G. Endrodi, Z. Fodor, S. Katz, and K. Szabo, JHEP **1104**, 001 (2011).
- [64] C. S. Fischer, J. Luecker, and C. A. Welzbacher, Phys.Rev. **D90**, 034022 (2014).
- [65] J. Cleymans, B. Kampfer, M. Kaneta, S. Wheaton, and N. Xu, Phys.Rev. **C71**, 054901 (2005).
- [66] F. Becattini, J. Manninen, and M. Gazdzicki, Phys.Rev. **C73**, 044905 (2006).
- [67] A. Andronic, P. Braun-Munzinger, and J. Stachel, Phys.Lett. **B673**, 142 (2009).
- [68] F. Becattini *et al.*, Phys.Rev.Lett. **111**, 082302 (2013).
- [69] J. Stachel, A. Andronic, P. Braun-Munzinger, and K. Redlich, J. Phys. Conf. Ser. **509**, 012019 (2014).
- [70] A. Andronic, Int. J. Mod. Phys. **A29**, 1430047 (2014).
- [71] P. Alba *et al.*, Phys.Lett. **B738**, 305 (2014).
- [72] A. Bzdak, V. Koch, and V. Skokov, Phys.Rev. **C87**, 014901 (2013).
- [73] F. Karsch, K. Morita, and K. Redlich, (2015), 1508.02614.
- [74] STAR Collaboration, L. Adamczyk *et al.*, Phys.Rev.Lett. **112**, 032302 (2014).
- [75] STAR Collaboration, L. Adamczyk *et al.*, Phys.Rev.Lett. **113**, 092301 (2014).
- [76] STAR, M. M. Aggarwal *et al.*, (2010), 1007.2613.
- [77] V. Skokov, B. Friman, and K. Redlich, Phys.Rev. **C88**, 034911 (2013).
- [78] P. Alba *et al.*, (2015), 1504.03262.
- [79] M. Nahrgang, M. Bluhm, P. Alba, R. Bellwied, and C. Ratti, (2014), 1402.1238.
- [80] A. Andronic, P. Braun-Munzinger, and J. Stachel, Nucl.Phys. **A772**, 167 (2006).